Marine and Petroleum Geology 46 (2013) 190–200

Contents lists available at SciVerse ScienceDirect

Marine and Petroleum Geology

journal homepage: www.elsevier.com/locate/marpetgeo

Chemostratigraphy of deep-sea Quaternary sediments along the Northern Gulf of Mexico Slope: Quantifying the source and burial of sediments and organic carbon at Mississippi Canyon 118

Wesley C. Ingram [a,*], Stephen R. Meyers [b,1], Christopher S. Martens [a]

[a] University of North Carolina – Chapel Hill, Department of Marine Sciences, 3202 Venable Murray Hall, CB 3300, Chapel Hill, NC 27599-3300, USA
[b] University of North Carolina – Chapel Hill, Department of Geological Sciences, Mitchell Hall, CB 3315, Chapel Hill, NC 27599-3315, USA

ARTICLE INFO

Article history:
Received 22 September 2012
Received in revised form
15 April 2013
Accepted 7 May 2013
Available online 5 June 2013

Keywords:
Gulf of Mexico
Chemostratigraphy
Sedimentary geochemistry
MC118
XRF
Cold seeps

ABSTRACT

This study investigates late Pleistocene to Holocene sedimentation, sedimentary geochemistry, and organic-carbon burial near the Mississippi Canyon 118 (MC118) gas-hydrate and cold-seep field at 890 m water depth – the first National Gas Hydrate Seafloor Observatory. The depositional history is reconstructed, producing a paleoenvironmental context for ongoing geochemical and geophysical monitoring at MC118. A chemostratigraphy is established from sediments that were recovered in 10 shallow gravity cores surrounding the MC118 field on the Northern Gulf of Mexico Slope. Geochemical data (from X-ray fluorescence core scanning, CO_2 coulometry, and inductively coupled plasma emission spectrometry) are evaluated within the context of a detailed chronostratigraphy to map geochemical burial fluxes across MC118 during distinct stratigraphic intervals, each of which represents substantial changes in the depositional environment. These measurements are accompanied by Rock Eval pyrolysis data to aid in the evaluation of organic matter source contributions.

The new dataset provides a means to quantitatively assess temporal and spatial changes in geochemistry and deposition surrounding the MC118 field. Results indicate that terrigenous sediment burial flux is the primary control on temporal changes in sediment composition and organic carbon burial, which are linked to sea level change and Mississippi delta lobe switching. Terrigenous proxy burial fluxes (titanium and insoluble residue) and organic carbon accumulation (primarily "type III" organic matter) are elevated during the interval spanning 14 to 9.5 kilo-years BP, compared to more recent deposition at MC118. Conversely, $CaCO_3$ accumulation (due to pelagic biogenic sources) is more consistent through time, although $CaCO_3$ concentration displays pronounced changes due to variable dilution by clay. The gas-hydrate and cold-seep field itself forms a bathymetric high due to salt diapirism, which is reflected in spatial patterns recorded in the chemostratigraphy. Analyses of geochemical burial fluxes indicate an increase of all sedimentary components (pelagic and terrigenous, including total organic carbon) with increased distance from the field. The results suggest a relatively stable spatial pattern of sedimentation with respect to MC118 during the latest Pleistocene and Holocene, but also a dynamic nature of deposition near the salt diapirism-induced bathymetric high, which contains the present day gas-hydrate deposits and active cold seeps.

1. Introduction

The Mississippi Canyon 118 (MC118) gas-hydrate and cold-seep field is situated on the northern Gulf of Mexico slope in approximately 890 m water depth, 150 km south of Gulfport Mississippi (Fig. 1). This study investigates the chemistry of late Pleistocene to Holocene deep-sea sediments surrounding the MC118 field, to evaluate controls on organic matter burial, reconstruct depositional history, and provide a paleoenvironmental context for ongoing geochemical and geophysical monitoring (Macelloni et al., 2010, 2012; Lapham et al., 2008; McGee, 2006). This new geochemical dataset is integrated with a recently published chronostratigraphy at MC118 (Ingram et al., 2010) to specifically address the following inter-related research questions: (1) How have terrigenous and pelagic inputs, including organic matter burial,

---

[*] Corresponding author. Present address: Weatherford Laboratories, 16161 Table Mountain Parkway, Golden, CO 80403, USA. Tel.: +1 850 591 1392.
E-mail address: wesley.ingram@weatherfordlabs.com (W.C. Ingram).
[1] Present address: University of Wisconsin–Madison, Department of Geoscience, Weeks Hall, 1215 West Dayton Street, Madison, WI 53706, USA.

0264-8172/$ – see front matter © 2013 Elsevier Ltd. All rights reserved.
http://dx.doi.org/10.1016/j.marpetgeo.2013.05.004

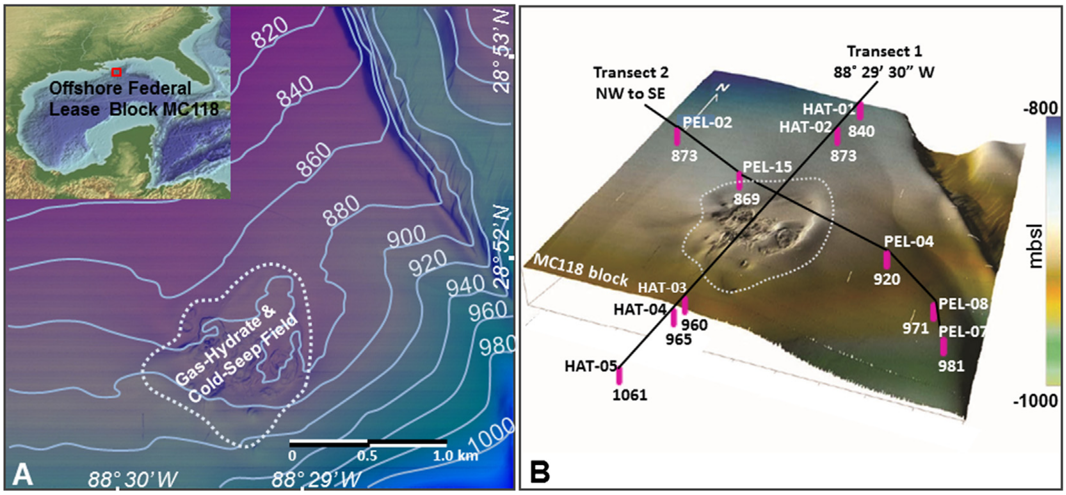

Figure 1. *Panel A*: Bathymetric map of the study area (Block MC118) with labeled contours (light blue) in meters water depth (base map courtesy of Ken Sleeper) with inset digital elevation and bathymetry map (top left; NOAA geophysical data center image) of the Gulf of Mexico Region. Bathymetry provided by the Gulf of Mexico Hydrate Research Consortium (modified after Sleeper et al., 2006). The location of MC118 offshore federal lease block is indicated by the red box in the inset map. The extent of the studied gas hydrate-cold seep field is outlined by the dotted line and is characterized by an area with gas vents, seafloor pockmark features, petroleum seepage, shallow faults, carbonate hard-grounds and gas hydrate deposits. *Panel B*: Bathymetric map of the study site with the location of cores collected during cruises on the R/V *Hatteras* and R/V *Pelican*; base map image is courtesy of the Gulf of Mexico Hydrate Research Consortium. Cores are indicated as vertical magenta lines, with core identification (above) and water depth (in meters) below the core symbol. The edge of the gas hydrate-cold seep field is outlined by a thin dotted white line, black lines connect core symbols and indicate transects onboard the R/V *Hatteras* ("Hatteras Transect") and R/V *Pelican* ("Pelican Transect"). The color bar on the far right indicates water depth. (For interpretation of the references to color in this figure legend, the reader is referred to the web version of this article.)

varied during the late Pleistocene and Holocene at MC118?, (2) How have global sea-level changes and regional factors such as delta-lobe switching influenced deposition during this period?, and (3) What is the influence of the gas-hydrate and cold seep field – including seafloor warping associated with salt diapirism – on temporal and spatial changes in pelagic and terrigenous sedimentation over the studied area?

To address these research questions, a multi-proxy geochemical approach is employed. X-ray fluorescence (XRF) core scanning (Richter et al., 2006) is conducted on a total of 10 shallow gravity cores strategically distributed across the seafloor (Ingram et al., 2010, Fig. 1), to generate nearly continuous down-core profiles of Al, Ti, K, Si, Fe and Ca. High resolution (cm scale) XRF core scans (counts) are calibrated to concentration data using Inductively Coupled Plasma Atomic Emission Spectrometry (ICP-AES; wt.% Al, Ti, K, Si, Fe, Ca) and CO_2 Coulometry (wt.% $CaCO_3$; Huffman, 1977). These measurements are supplemented by wt.% Total Organic Carbon (TOC) and wt.% insoluble residue from CO_2 coulometry and Rock Eval pyrolysis data for organic matter typing. This new geochemical dataset is integrated with the MC118 chronostratigraphy established by Ingram et al. (2010), to evaluate spatial and temporal variability of burial fluxes for key geochemical components. The elemental proxies used herein reflect pelagic and terrigenous contributions ($CaCO_3$, Ti, insoluble residue) as well as organic carbon burial (TOC accumulation). In total, the study comprises 33,849 unique geochemical measurements, providing an extensive documentation of sediment geochemistry, and an important context for ongoing monitoring at the first National Gas Hydrate Seafloor Observatory (as designated by the US Department of Energy; McGee, 2006).

1.1. *Geologic setting: MC118*

The MC118 field is the focus of an extensive multi-disciplinary effort to document physical and biogeochemical processes associated with gas hydrates and marine hydrocarbon systems, as part of a larger consortium effort (Simonetti et al., 2013; Lutken et al., 2006; Sassen et al., 2006). The field is located on the upper continental slope of the northern Gulf of Mexico, centered at 28.8523°N and 88.4920°W, at approximately 890 m depth along an overall gently sloping seafloor. Locally, the seafloor within the vicinity of the hydrate and cold seep field is influenced by numerous factors including gas hydrate formation, hydrocarbon (gas and petroleum) seepage and apparent seafloor warping from shallow salt deposits. Visible outcroppings of gas hydrates, faulted carbonate "hard-grounds" and pockmark features consistent with gas and petroleum seepage cover approximately 1 km^2 of the seafloor (Sassen et al., 2006; Sleeper et al., 2006; Macelloni et al., 2010, 2012). While the seaward slope across the study area typically ranges from 3° to 4°, slopes of 10° to 12° are present locally across the area of gas-hydrate formation and cold seepage where pockmarks exists (Sleeper et al., 2006).

Regionally, the bathymetry of the Gulf of Mexico continental slope is heavily influenced by the extensive Louann (Jurassic in age) salt formation (Diegel et al., 1995; Galloway et al., 2000; Jackson, 1995). Deformation of salt within the basin has contributed to the present-day hummocky bathymetry of the northern Gulf of Mexico slope (Jackson, 1995). At MC118, a salt diapir lies approximately 300 m below the ocean floor and is a probable migration pathway for light hydrocarbons sourced by "leaky" reservoirs at depth (Macelloni et al., 2012), such diapirs are prolific along the northern Gulf-of-Mexico slope (McBride, 1998).

Ingram et al. (2010) document the lithostratigraphy, biostratigraphy, and chronostratigraphy for MC118 using the same core material as in the present study. Previous analysis identified four stratigraphic intervals: Unit IA, Unit IB, Unit II, and Unit III (Fig. 2), which also follow distinct changes in chemostratigraphy (Fig. 3). Stratigraphic "Unit IA" is a massive, calcareous nannofossil clay and is Late Holocene (2.3 Ka to present) in age (Fig. 2). Unit IA is defined at its top by the shallowest recovered sediment (core tops), and at its base by the onset of a more $CaCO_3$-rich interval (defining the sub-adjacent "Unit IB"). The higher clay content of Unit IA, while not obvious from visual description, is apparent from published Ca/Ti XRF scans (Ingram et al., 2010). Sediments of Unit IA are relatively thin and extend to 38 cmbsf at its greatest (HAT-02) to less than 5 cm at its shallowest (HAT-03, PEL-04, -15 and -08). At the most

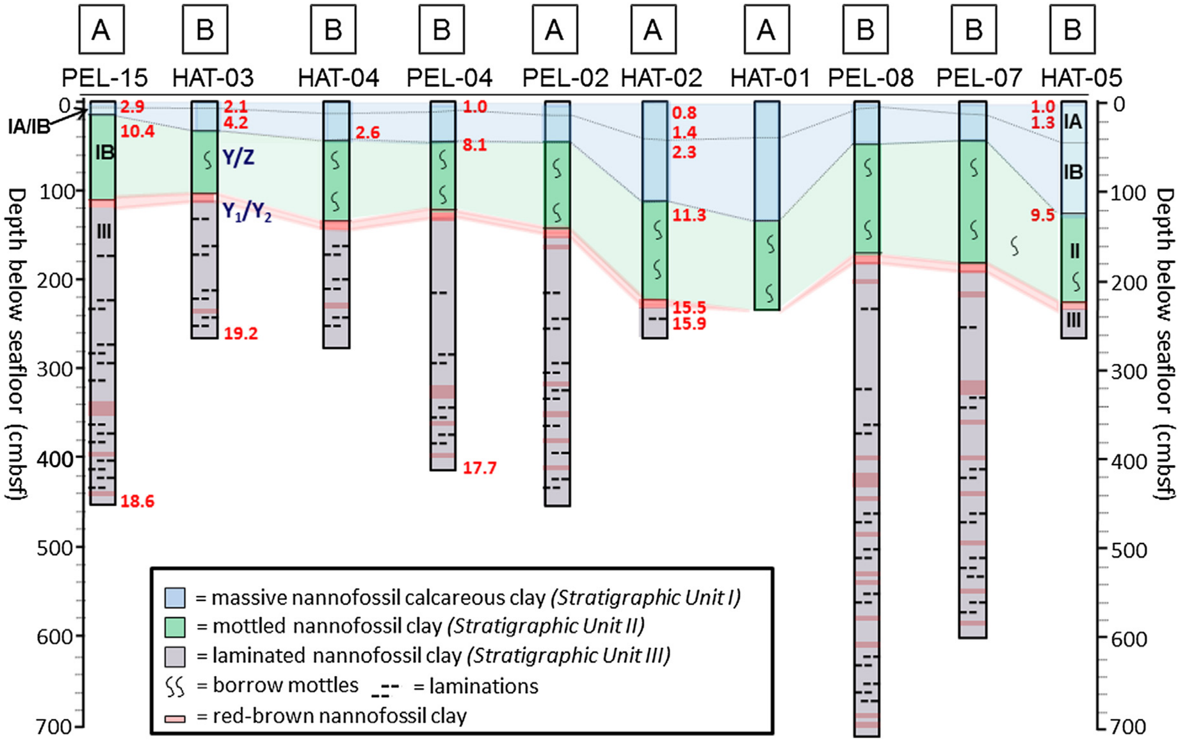

Figure 2. Stratigraphic correlation of marine sediments collected across the MC118 study area. Cores are arranged by increasing distance (left to right) from the gas hydrate-cold seep field. The "A" and "B" designations at the top of each core indicate whether the site is located above or below (respectively) the seep field. Dates obtained via AMS radiocarbon analysis of planktonic foraminifera (red, Ka) and foraminiferal biostratigraphic boundaries (dark blue, Y/Z ~ 10 Ka and Y_1/Y_2 ~ 15 Ka) are shown alongside their stratigraphic position; all reported ages are in calendar kilo-years BP. Three distinct stratigraphic units are identified as follows: Unit I (light blue) = massive nannofossil calcareous clay; Unit II (light green) = mottled nannofossil clay; Unit III (gray) = laminated nannofossil clay containing reddish-brown nannofossil clay layers (red lines). A distinct ~5-cm thick reddish clay layer with highly "reworked" (pre-Quaternary) nannofossils defines the top of Unit III. (For interpretation of the references to color in this figure legend, the reader is referred to the web version of this article.)

"expanded" core sites, Unit IA includes an additional minor and shallower increase in carbonate content, which is visible in Cores HAT-02 and HAT-05 (Fig. 4 in Ingram et al., 2010, Fig. 5). This minor "peak" occurs at approximately 10–15 cmbsf in the two cores and implies variability in the lithogenic/pelagic inputs in shallow (most recent) Late Holocene sediments (see Discussion). Stratigraphic "Unit IB" the most carbonate-rich unit, is a massive calcareous nannofossil clay, and is also Holocene (9.5–2.3 Ka) in age (Fig. 2; Ingram et al., 2010). Sediments of this unit are thicker (18–83 cm) than the shallower Unit IA and extend down to a maximum depth of 120 cmbsf (Fig. 2).

The shallower Units IA and IB, approximately Holocene (9.5 Ka to present) in age, are markedly different than subjacent units. Below these younger sediments lies "Unit II", a mottled nannofossil clay with substantially less carbonate, of late Pleistocene to earliest Holocene in age (14–9.5 Ka). The base of Unit II is defined by a distinct reddish-brown colored band ("red band") composed of pre-Quaternary nannofossils, which have been linked to melt water pulse 1A (Marchitto and Wei, 1995), and thus provides a chronostratigraphic horizon (dated between 14 and 15 kilo-calendar years; Ingram et al., 2010). The "red band" ranges in depth from 115 cm to 255 cmbsf at MC118 and also marks the top of the deepest stratigraphic unit. This lowermost interval, Stratigraphic "Unit III", is a well-laminated, nannofossil clay, and is late Pleistocene (>14,000 years) in age (Fig. 2; Ingram et al., 2010). It is similar to Unit II as it is also carbonate poor relative to Units IA and IB. The unit displays reddish banding that increases in frequency with depth (Fig. 2). Unit III has no defined chronostratigraphic base, and thus extends down to the deepest recovered sediments, at 711 cmbsf in Core PEL-08.

1.2. The marine sedimentary geochemistry archive

Numerous geochemical proxies are utilized in the present study, and thus a brief review relevant to their application at MC118 is provided in this section. Several elements K, Al, Ti (Fig. 3) serve as lithogenic indicators in the hemipelagic deposits at MC118, and are derived from terrigenous alumino-silicate clays and silts (Kujau et al., 2010; Pattan et al., 2005). Titanium exists in low concentrations (<1%) in marine sediment, yet it is also relatively chemically unreactive in such settings, providing a particularly robust "conservative" lithogenic indicator. In the Gulf of Mexico, titanium is primarily derived from ilmenite ($FeTiO_3$), closely followed by rutile (TiO_2), minerals associated with sand- and silt-size grains (Appelbaum and Bouma, 1972; Woolsey, 1984). Ingram et al. (2010) established that lithogenic sand-sized grains are not readily apparent in shallow MC118 sediments, thus titanium inputs are likely fine-grained silts. The elements Fe and Si are also potential indicators of lithogenic inputs at MC118, yet can be substantially influenced by authigenic processes and/or pelagic biogenic inputs along continental slope settings (Kasten et al., 1998; DeMaster, 1981).

It is generally assumed that the $CaCO_3$ content in deep marine sediments is primarily derived from biogenic skeletal material such as tests of calcareous nannoplankton, foraminifera and pteropods (Bralower and Thierstein, 1987; Sageman and Lyons, 2004). The use of wt.% $CaCO_3$ as a measure of pelagic biogenic carbonate contribution is most useful at oceanographic sites well above the lysocline, and localities where diagenetic carbonate dissolution is not substantial. The detailed sedimentologic and biostratigraphic evaluation of MC118 sediments by Ingram et al. (2010) revealed no evidence for authigenic carbonate (or dissolution) in the 10 studied

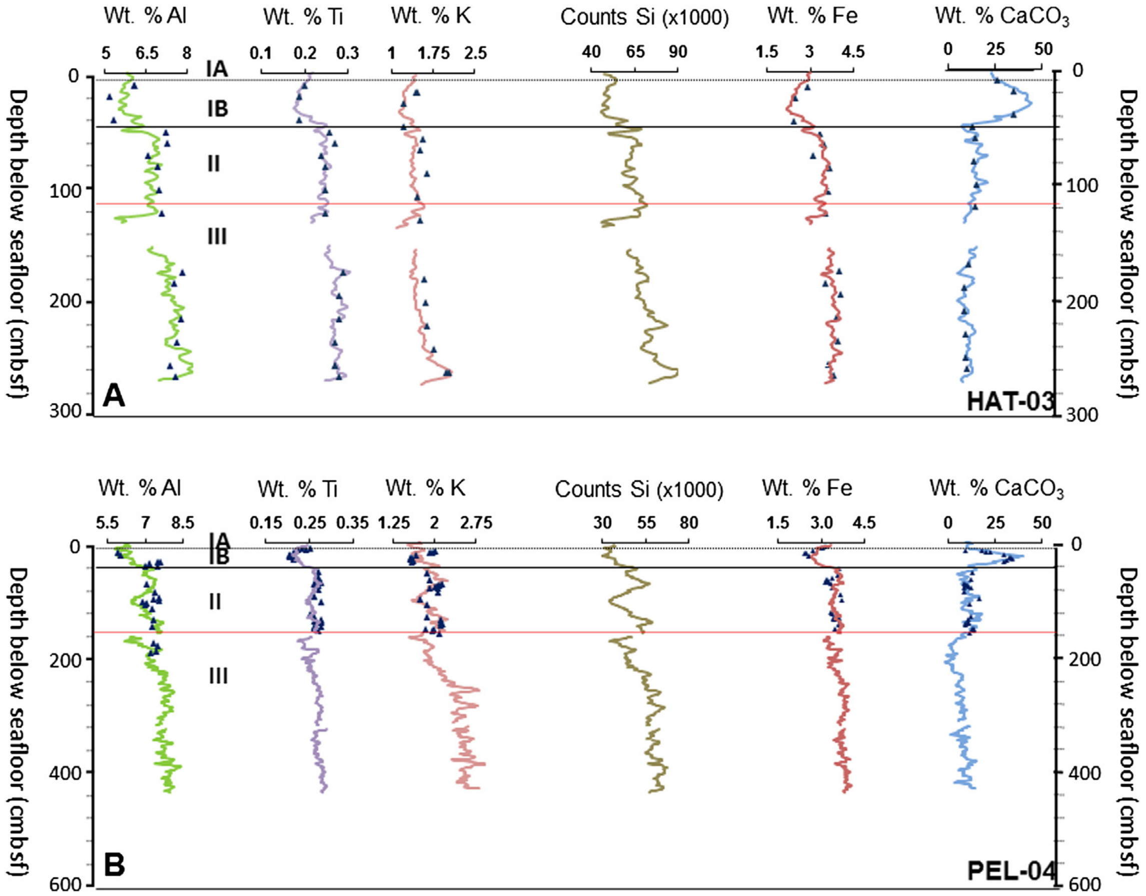

Figure 3. *Panel A* (top): XRF results (calibrated and un-calibrated) for Core HAT-03. From left to right: Al, Ti, K, Si, Fe and $CaCO_3$. The above calibrated and un-calibrated XRF core scans are smoothed using a 3-point moving average (Si is un-calibrated). Stratigraphic Units IA, IB, II and III are as described in the text. *Panel B* (bottom): same as above, for Core PEL-04 and with a condensed depth scale (0–600 cmbsf).

cores. While authigenic carbonates form at cold seeps (Bian et al., 2013), MC118 cores are removed from the vicinity of present-day gas hydrate formation and cold seepage; hence seep carbonates are not apparent. Hence wt.% $CaCO_3$ should be a reliable pelagic biogenic indicator at MC118. Finally, the accumulation of organic carbon (TOC) is also associated with multiple sources, and refractory terrestrial organic matter can even dominate along “deltaic” continental margins (Snowdon and Meyers, 1992), which may be the case at MC118 (see Discussion).

2. Methods

2.1. Core collection and processing

Sediment gravity coring was conducted from the surface ships R/V *Hatteras* in August 2007 and R/V *Pelican* in April 2008. Five cores were recovered by the R/V *Hatteras* in a depositional dip orientation, and five additional cores were collected onboard the R/V *Pelican* along a NW to SE transect (Fig. 1). For details of shipboard and land-based core collection and processing methods see Ingram et al. (2010) and Sleeper and Lutken (2008).

2.2. X-ray fluorescence core scanning and calibration

Cores were analyzed using an Avaatech-XRF core scanner (Richter et al., 2006) with an Oxford 50 W X-ray source (rhodium target), and a Canberra X-PIPS detector with a 1500-μm silicon crystal. Continuous XRF scanning was conducted at 1-cm resolution and was used to evaluate changes in the bulk geochemical composition of MC118 sediments, with a focus on the elements Ca, Al, Si, K, Ti, and Fe (Fig. 3). Analysis of these elements was based on both their analytical reproducibility and their utility as proxies for sedimentary inputs (biogenic vs. lithogenic). The elements Ca, Al, and Si were measured using a 5 kV source voltage, 900 mA, without a filter, using a 90 s measurement time. Heavier elements, K, Ti and Fe were measured using a 10 kV source voltage, 1000 mA, with a cellulose filter, using a 90 s measurement time. To quantify reproducibility, duplicate scans were performed at 10-cm resolution using the same scanning parameters (Table 1).

Sediment samples from cores were collected to measure wt.% composition of the studied elements to calibrate XRF data (counts) to down-core concentration profiles. Samples were taken at numerous stratigraphic intervals to span the full range of geochemical variability detected using the XRF core scanning. All samples were prepared by extracting 1-cm thick intervals of the un-scanned core half, which were then placed in 100-mL beakers, dried at 50 °C for 48 h, and pulverized to a 100 mesh (<0.064 mm) fraction. Remaining dried and crushed sediments were placed into vials, and subsamples were taken from the homogenized powdered fraction for subsequent geochemical measurements via CO_2 coulometry and ICP-AES.

2.3. CO_2 coulometry, ICP-AES, and XRF calibration

Standard coulometry procedures (Huffman, 1977) were used to determine inorganic carbon (CO_3^{2-}), total organic carbon (TOC),

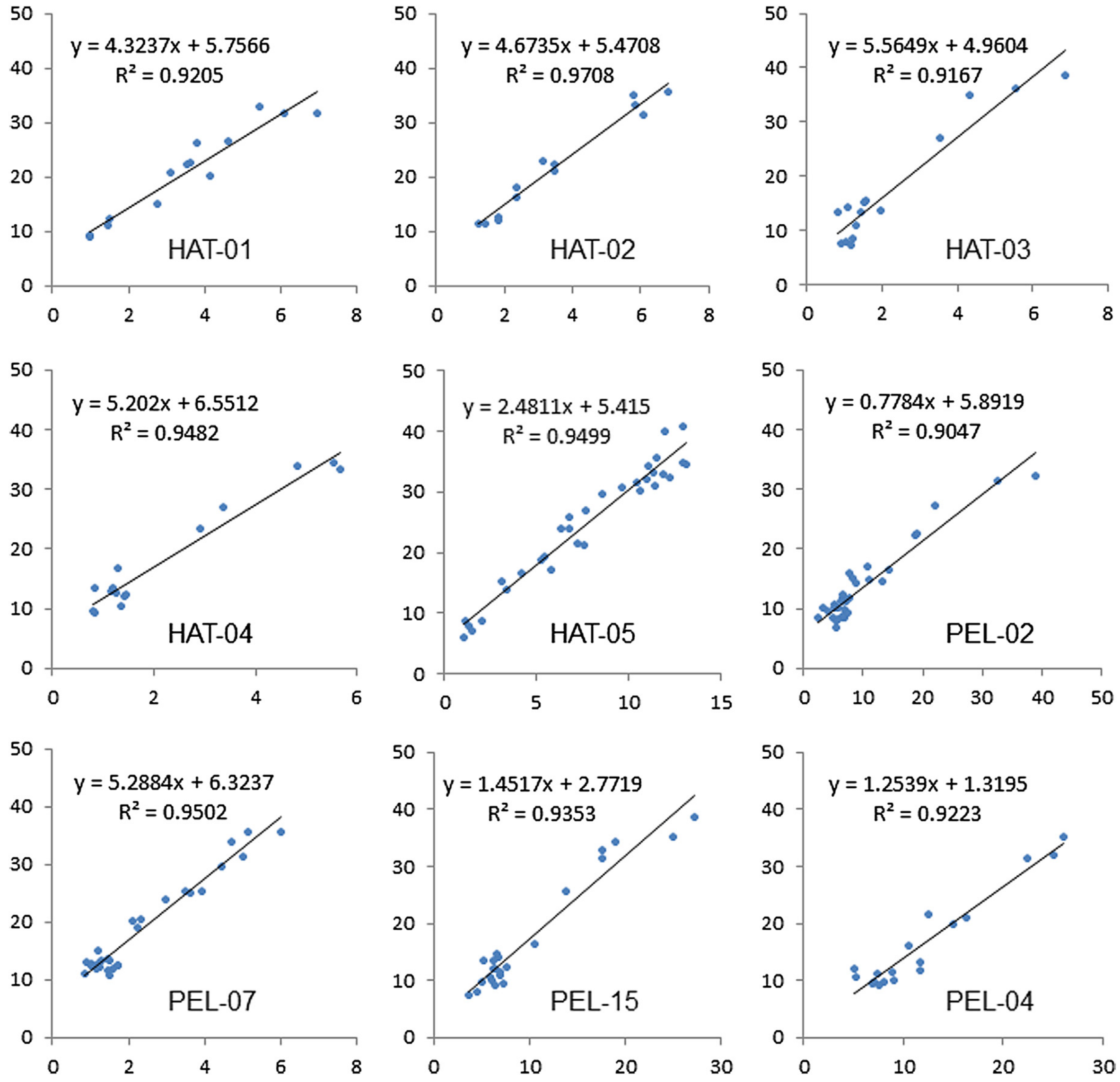

Figure 4. Cross plots of XRF Ca/Ti data (*x*-axis) and wt. % $CaCO_3$ measured using the CO_2 Coulometry acid digestion method (*y*-axis), for each of the nine calibrated cores. Correlation coefficients and least-squares linear fits for each calibration equation are also presented.

and insoluble clay (% residue) concentration. A total of 836 measurements, including duplicates, were performed on 9 cores using the acid digestion and combustion steps of the coulometry technique. Duplicate measurements of percent carbon for acid digestion and combustion measurements yield errors of less than 5% for inorganic carbon and less than 10% for organic carbon (coefficient of variation; Table 1). Percent total organic carbon (TOC) is calculated by subtracting the inorganic portion (CO_3^{2-}) from total carbon content. Weight percent $CaCO_3$ is calculated by multiplying percent inorganic carbon (from acid digestion) by the stoichiometric conversion (8.333), assuming all carbonate is present as either calcite or aragonite. Insoluble residue (primarily clay and silt) is determined as the residual percentage after accounting for TOC and $CaCO_3$.

Calibration equations (least-squares linear fits) for conversion of the XRF data (counts) to wt. % $CaCO_3$ are displayed in Figure 4. The ratio of Ca/Ti was found to provide a better predictor of wt. % $CaCO_3$ than Ca counts. This is likely due to correction for minor changes in bulk density, which influence both Ca and Ti XRF measurements. While the calibration results are excellent, some disagreement is expected given that the two analytical methods are measuring somewhat different sample substrates: CO_2 coulometry is conducted on a homogenized powder from a 1-cm thick interval with a volume of approximately 10 cm^3, and the XRF analysis is conducted over a 1-cm^2 area of the split-core surface with detection effective to a depth of $<$100 microns for light elements.

In addition, sediment samples from two cores, one from each transect (HAT-03 and PEL-04), were selected to calibrate XRF scans using ICP-AES (SGS Laboratory, Toronto). Crushed sediment samples were prepared following the procedure outlined in Section 2.2, and analyzed for a suite of elements using a multi-acid digestion (HF, HNO_3, HCl) (Table 2). For a detailed explanation of the method (major and trace elements in rocks and sediments) see Murray et al. (2000). Duplicate measurements from the MC118 cores yield low errors of 0.7–1.8% (coefficient of variation), depending upon the specific element and core investigated (Table 1). A summary of derived calibration equations (least-squares linear fits) are provided for conversion of XRF count data to mass composition (Table 2).

2.4. Rock-Eval pyrolysis

Ten powdered dried sediment samples were analyzed using a Source Rock Analyzer (SRA) by Weatherford Geochemistry

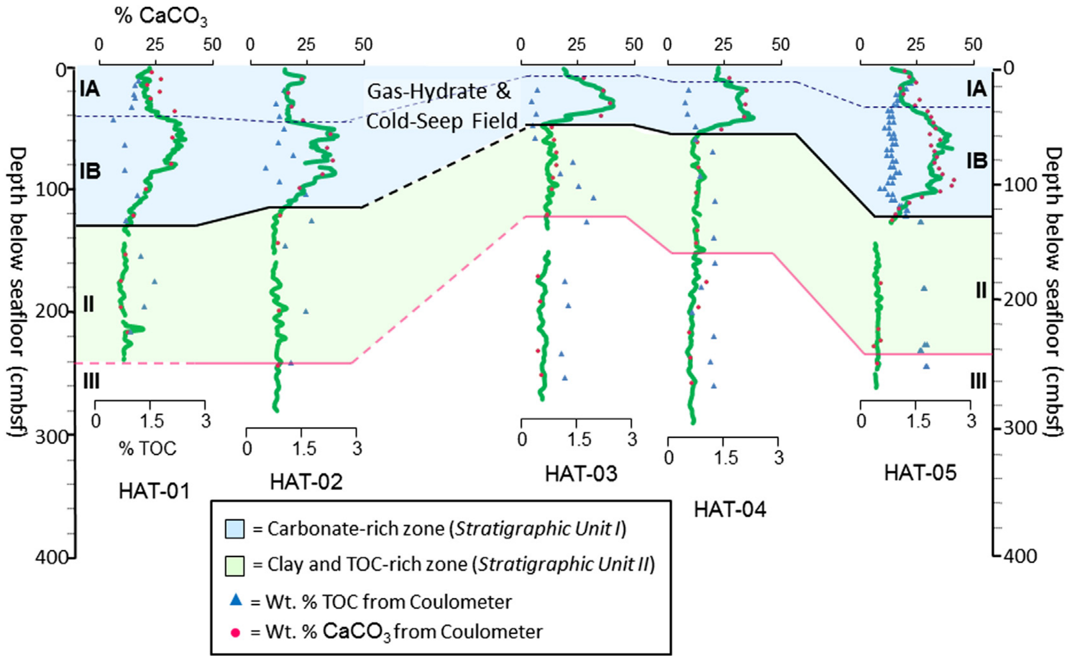

Figure 5. Calibrated weight percent calcium carbonate (solid green curves) derived from XRF scanning of cores from the Hatteras Transect (Figs. 1, 2). The data represented by the green curves are smoothed using a 3-point moving average. Total organic carbon (blue triangles) and wt. % $CaCO_3$ (red dots) from CO_2 Coulometry (see legend) are also plotted. Stratigraphic Units IA, 1B, II and III are as defined in the text. (For interpretation of the references to color in this figure legend, the reader is referred to the web version of this article.)

Laboratory in Houston, TX to determine the type of organic matter deposited under changing sedimentation regimes. The samples are from core HAT-03, and span all stratigraphic units (IA, IB, II and III). Determination of the pyrolysis combustion peaks is similar to prior generation instrumentation (Claypool and Reed, 1976; Espitalié et al., 1985). In summary, pyrolysis peaks are as follows: (S1) measures free hydrocarbons (volatile bitumen), (S2) hydrocarbons cracked during programed pyrolysis, (S3) oxygen content of the organic matter. Rock pyrolysis using the SRA method may encounter problems with respect to TOC determination when dealing with unstable carbonates volatilized at low temperatures (Espitalié et al., 1985); for this reason along with elevated carbonate concentrations in MC118 sediments, CO_2-coulometry TOC values are considered more reliable, and were used in all calculations.

2.5. Bulk density determination and mass accumulation rates

Sediment dry-bulk density is determined by following a procedure used by Dadey et al. (1992); they provide a correction for marine sediments with saline pore fluids. The following calculation is used (Dadey et al., 1992): $M_s = M - M_f = (M_d - s^*M)/(1 - s)$, where M = wet mass, M_s = corrected dry mass, M_f = pore-fluid mass, M_d = dry mass uncorrected and s = salinity (0.035). The mass accumulation rate (or "burial flux") for each geochemical proxy of interest is determined by multiplying the dry bulk density (g/cm^3), sedimentation rate (Ingram et al., 2010), and average concentration for each stratigraphic unit (IA, IB and II) at individual core sites. Rates were calculated for proxies diagnostic of biogenic ($CaCO_3$) and terrigenous inputs (Ti, insoluble clay; Fig. 7), as well as for organic carbon. Uncertainty of the burial fluxes was estimated by calculation of one standard deviation between maximum and minimum flux values (see error bars in Fig. 7). The maximum and minimum flux values were determined by combining variability in concentration of each proxy from duplicates with a chronologic error of 216 (+/−) calendar years, which was the maximum error encountered from AMS C-14 dating (Table 2 in Ingram et al., 2010).

3. Results

The four stratigraphic intervals (Unit IA, IB, II, III) spanning a 14 kilo-year record, previously described by Ingram et al. (2010), are considered here (see Section 1.1). The new dataset quantifies pronounced changes in wt. % $CaCO_3$, lithogenic elements, and TOC (Table 1; Figs. 3, 5–6). The most obvious feature at all core sites is a substantial reduction in wt.% Fe, K, Al, Si and Ti and organic carbon content during deposition of Unit IB (9.5–2.3 ka), associated with elevated wt.% $CaCO_3$ content (Figs. 3, 5–6). In contrast, Unit II (14–9.5 ka) and Unit III (>14 ka) are the most enriched in lithogenic elements and organic carbon. Based on this compositional data, the depositional history at MC118 can be characterized as one progressing from more organic-carbon and clay-rich during the latest Pleistocene, to more carbonate-rich and organic carbon-poor during the early-mid Holocene (9.5–2.3 ka). A reversal of this trend is observed in latest Holocene sediments of Unit IA (2.3 ka – present). This reversal is most apparent at core sites farthest from the MC118 field (HAT-01, -02 and -05; Figs. 1, 5), which also display a transient increase ("pulse") in wt.% $CaCO_3$ at some sites (HAT-02 and -05; Fig. 5). A summary of the geochemical results is presented in Table 1, and these data are also used in burial flux calculations of select geochemical proxies (Fig. 7). Mass accumulation rates (burial fluxes) are estimated using the chronostratigraphy of Ingram et al. (2010), concentrations of geochemical proxies ($CaCO_3$, TOC, Ti and Residual Clay; Table 1), and average bulk density measurements for each unit (1.716 g/cm^3 for Unit I) and (1.828 g/cm^3 for Unit II).

3.1. Geochemical mass accumulation rates

The mass accumulation rate of bulk sediment is characterized by a general increase with distance from the gas-hydrate and cold-seep field (Fig. 7A). However, core sites above the field often display elevated rates for a given distance, as compared to sites below the field (Fig. 7A), a feature that is especially obvious for Unit II and Unit IB. At all sites, the mass accumulation rate of bulk

Table 1
(A) Average coefficient of variation (CV) for each geochemical proxy considered in this study (Cores HAT-03 and PEL-04) based on duplicate analyses from each method, (1) X-ray fluorescence (XRF), (2) Inductively Coupled Plasma Atomic Emission Spectrometry (ICP-AES) and (3) CO_2 coulometry (CO_2). For the samples (N) column, values to the left are number of duplicates from XRF, values to the right are number of duplicates from ICP, and for TOC and $CaCO_3$ (with only one value) number of duplicates from CO_2 coulometry are indicated. (B) Average concentration values (wt.%) are determined for each proxy and used to determine mass accumulation rates (see Fig. 7) across each respective stratigraphic time interval, Unit IA, IB, II, and for the combined 14-ka record (Units I&II). (C) The range of values from CO_2 coulometry data for wt.% $CaCO_3$, TOC and insoluble residue, along with wt.% Ti from calibrated XRF scans.

Proxy	XRF CV	ICP-AES CV	CO_2–C CV	Samples (N)
(A) Average coefficient of variation				
Al	0.038	0.012	NA	52|6
Ti	0.049	0.018	NA	52|6
K	0.037	0.012	NA	52|6
Fe	0.020	0.007	NA	52|6
Ca	0.024	0.009	NA	52|6
TOC	NA	NA	0.087	20
$CaCO_3$	NA	NA	0.037	20

Core	Proxy	Unit IA	Unit IB	Unit II	Units I&II
(B) Average concentrations by interval					
HAT-03	wt.% $CaCO_3$	19.21	26.58	12.56	18.94
	wt.% TOC	0.36	0.26	1.19	0.73
	wt.% Ti	0.21	0.20	0.24	0.22
	wt.% insoluble residue	80.41	73.15	86.24	80.31
PEL-04	wt.% $CaCO_3$	12.79	25.39	11.06	14.67
	wt.% TOC	0.95	0.81	1.37	1.10
	wt.% Ti	0.24	0.22	0.25	0.25
	wt.% insoluble residue	86.25	73.79	87.55	84.22
(C) Range of values each proxy by interval					
HAT-03	wt.% $CaCO_3$	NA	38.75–13.24	15.37–12.11	38.75–13.11
	wt.% TOC	NA	0.23–0.36	1.95–0.38	0.23–1.95
	wt.% Ti	0.22–0.20	0.26–0.16	0.26–0.22	0.26–0.16
	wt.% insoluble residue	NA	86.45–60.93	85.30–83.32	86.45–60.93
PEL-04	wt.% $CaCO_3$	16.08	35.05–18.88	18.37–9.05	35.05–9.05
	wt.% TOC	0.95	1.04–0.50	1.79–1.38	1.79–0.5
	wt.% Ti	0.25–0.23	0.24–0.20	0.29–0.24	0.29–0.20
	wt.% insoluble residue	82.95	80.27–64.26	89.41–80.20	89.41–64.26

Table 2
Calibration equations (least-squares linear fits) for each element. These equations were used to convert XRF counts into weight percent composition (wt. %). The correlation coefficients and number of samples are also shown. See Figure 3 for graphical representation of ICP data plotted with the calibrated XRF core scans, and Figure 4 for the wt.% $CaCO_3$ calibrations.

Core	Proxy	Calibration eqn.	R^2 Value	Samples (N)
XRF-ICP elemental calibration data				
HAT-03	Al	$y = 5*10^{-4}(x) + 3.3396$	0.7319	15
	Ti	$y = 6*10^{-6}(x) + 0.0847$	0.9222	15
	K	$y = 2*10^{-5}(x) + 0.435$	0.7643	14
	Fe	$y = 6*10^{-6}(x) + 0.589$	0.8941	16
	Ca	$y = 2*10^{-4}(x) - 1.4069$	0.9154	14
PEL-04	Al	$y = 7*10^{-4}(x) + 3.8955$	0.6754	30
	Ti	$y = 4*10^{-6}(x) + 0.1584$	0.8302	32
	K	$y = 8*10^{-5}(x) + 0.7941$	0.7449	30
	Fe	$y = 6*10^{-6}(x) + 1.0749$	0.8112	30
	Ca	$y = 3*10^{-5}(x) - 1.7188$	0.9232	32
ICP-CO_2 coulometry calibration data				
HAT-03	$CaCO_3$	$y = 0.932(x) + 1.6417$	0.9926	12
PEL-04	$CaCO_3$	$y = 0.884(x) + 1.9768$	0.9871	17

sediment during Unit II (14–9.5 ka) is markedly higher than Unit IA (2.3 ka-present) and Unit IB (9.5–2.3 ka). These general spatial and temporal patterns of sediment accumulation are also observed in the burial flux of organic carbon (Fig. 7C), titanium (Fig. 7B), and insoluble residue (Fig. 7B). In contrast, the temporal changes in mass accumulation rate of $CaCO_3$ (Fig. 7D) are often less pronounced, although spatial trends show some similarity. To further illustrate these differences, note that $CaCO_3$ accumulation rates vary from 4 to 50 g m^{-2} yr^{-1} across the seafloor in Unit IA (Fig. 7D), an increase by a factor of 12. However, $CaCO_3$ burial fluxes at any given core site demonstrate much less temporal variability (some sites yield almost no change such as HAT-01, -02 and -05; Fig. 7D). This contrasts with TOC burial fluxes, which exhibit much greater temporal variability (0.36–3.0 g m^{-2} yr^{-1} for HAT-03), as opposed to the spatial variability (0.32–1.8 g m^{-2} yr^{-1} within Unit IB), and this trend is also quite consistent across MC118 (Fig. 7C). Hence, the most important observation for $CaCO_3$ mass accumulation is that, despite substantial changes in sedimentation rate through the Late Pleistocene to the Holocene (Ingram et al., 2010), its burial flux is more stable, as compared to TOC burial flux which changes dramatically (Figs. 5–7).

The mass accumulation of lithogenic components (Ti and insoluble residue) exhibits similar spatial patterns and temporal changes as TOC burial flux (Fig. 7C). In other words, lithogenic components display dramatically increased burial during deposition of Unit II at all sites, and a pattern of generally higher burial fluxes at sites farther from the gas-hydrate and cold-seep field (Fig. 7C). Hence, while spatial heterogeneity is, at times, considerable at MC118, the temporal variability is even larger for lithogenic elements and replicated at every core site (Fig. 7).

3.2. Rock-Eval pyrolysis

Sediments spanning the late Pleistocene and Holocene at MC118 demonstrate markedly different T_{max} (ranging from 385 to 430 °C) and hydrogen index values. Samples from the Holocene (20–40 cmbsf) contain mixed type II/III kerogens, while those from the late Pleistocene to early Holocene (70–250 cmbsf) yield a type-III kerogen signature (Fig. 8). All samples are immature exhibiting low T_{max} values. These analyses suggest that organic matter within Unit II (14–9.5 ka) is predominantly comprised of type-III kerogens (Fig. 8).

4. Discussion

4.1. Pelagic versus terrigenous sedimentation

An important observation at MC118 is the stability of pelagic (marine biogenic) sedimentation as evident from the relatively consistent mass accumulation of $CaCO_3$ through time (Fig. 7) despite dramatic changes in down-core concentration of wt.% $CaCO_3$ (Figs. 5–6). For example, elevated $CaCO_3$ concentrations are a distinctive feature of Unit IB sediments (Figs. 5–6), yet this increase is not reflected in the $CaCO_3$ burial flux across this same interval (Fig. 7). In fact, the highest $CaCO_3$ accumulation rates almost uniformly occur within carbonate-poor Unit II (Fig. 7). Interestingly, the site with the most consistent rate of $CaCO_3$ accumulation across Units IA to II (49.7–51.8 g m^{-2} yr^{-1}, Core HAT-01) is located far upslope from the MC118 field (Figs. 1, 5, and 7). Despite the consistency of $CaCO_3$ accumulation here (Core HAT-01), there is still substantial changes in wt. % $CaCO_3$ across this same interval (11.1–25.6 wt. %; Fig. 5). It is reasonable to assume that this coring site is one of the least likely to be influenced by the field (or salt diapirism), due to its distal and upslope position from the seep site (Fig. 1). Thus, geochemical burial fluxes at this location (Core

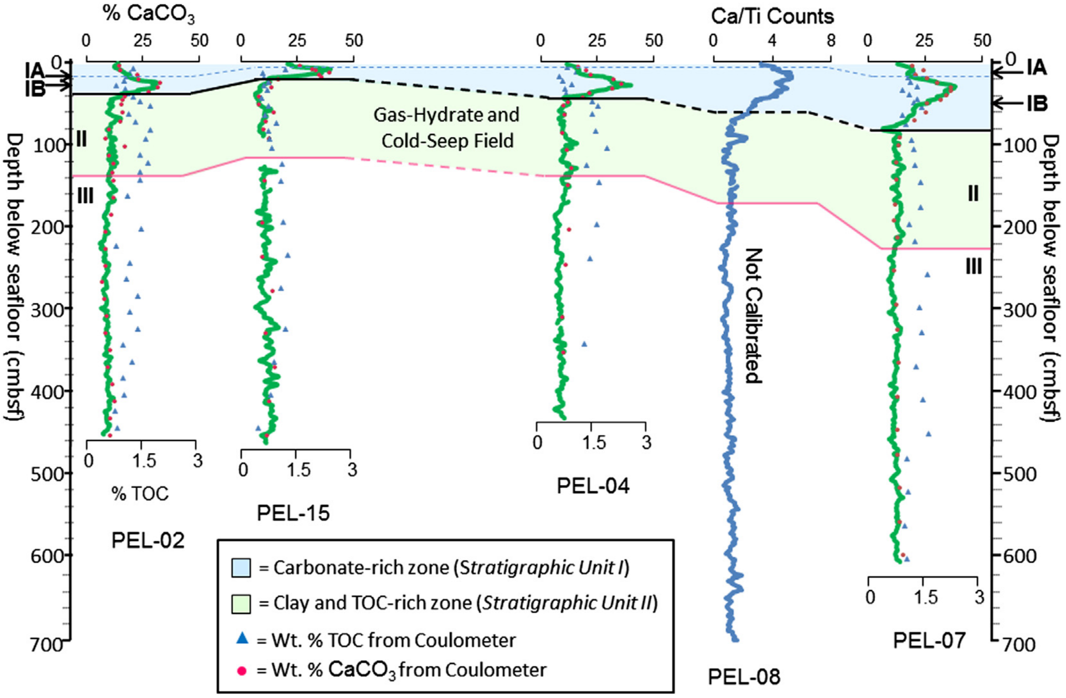

Figure 6. Calibrated weight percent calcium carbonate (solid green curve) derived from XRF scanning of cores from the Pelican Transect (Figs. 1, 2). The data represented by the and blue curves are smoothed using a 3-point moving average. Total organic carbon (blue triangles) and wt. % $CaCO_3$ (red dots) from CO_2 Coulometry (see legend) are also plotted. Stratigraphic Units IA, 1B, II and III are as defined in the text. (For interpretation of the references to color in this figure legend, the reader is referred to the web version of this article.)

HAT-01) most likely represent "background" sedimentation, undisturbed by process associated with the MC118 field or salt diapir (Ingram et al., 2010, Fig. 1).

The terrigenous lithogenic signal is documented at the MC118 site by titanium and insoluble residue accumulation (clay and silt inputs). Results indicate rapid lithogenic accumulation within Unit II (14–9.5 ka), followed by much slower accumulation rates during the later Holocene intervals (Unit IA and IB) (Fig. 7C). The reduction in accumulation of the lithogenic fraction is most likely tied to a retreating shoreline and diminished terrestrial influence at the site. This interpretation has been invoked to explain a similar trend at DeSoto Canyon (Winn et al., 1995), ~100 km to the east of MC118. In both locations along the eastern Gulf of Mexico Margin, glacial low-stands exposed parts of the shelf (Törnqvist et al., 2006), thereby increasing proximity to the shoreline and enhancing terrigenous sedimentation.

In summary, $CaCO_3$ burial flux (pelagic component of sedimentation) from the late Pleistocene-early Holocene interval (14–9.5 Ka) to the Holocene interval (9.5–2.3 Ka), was relatively stable despite considerable changes in depositional environment at MC118 associated with post-glacial sea-level rise (Fig. 7D). Thus, elevated $CaCO_3$-content in shallow (Unit IB) sediments is due to a reduction in the dilution effect from lithogenic inputs, and not from a substantial change in primary productivity. These results imply that primary production in the water column has remained relatively consistent in the northern Gulf of Mexico from the late Pleistocene to the Present, with perhaps slightly elevated carbonate production during the latest Pleistocene (Fig. 7D). In contrast, changes in lithogenic inputs appear to be the controlling factor on chemical composition of sediments. It is reasonable to conclude that post-glacial sea-level rise and Mississippi Delta lobe shifting drove changes in bulk geochemistry of recent sediments at MC118 by modifying terrigenous sedimentation (lithogenic inputs). The supply of lithogenous sediments to MC118 are clays and silts eroded from the Mississippi drainage basin or delta, which are then discharged into the Northern Gulf of Mexico. It has been shown that the suspended sediment load (siliciclastic material) from the Mississippi River is initially deposited within 30 km offshore from the delta, then can disperse across the shelf over a much larger area by storms and wave energy (Corbett et al., 2004; Gordon and Goni, 2004). Silt and sands are potentially remobilized (including turbidity flows) farther down the Gulf-of-Mexico Slope where they may accumulate in seafloor depressions or at MC118 yet sand-sized grains were not observed here (Prather et al., 1998; Winkler, 1996).

4.2. *Organic matter type and burial*

The spatial and temporal patterns of organic matter burial at the study site are clearly influenced in a way similar to overall sedimentation (Fig. 7A; Ingram et al., 2010), particularly the lithogenic components (Figs. 3 and 7D). The MC118 record exhibits TOC concentrations that are substantially lower in early-late Holocene Units IA (2.3 ka-present) and IB (9.5–2.3 ka) as compared to late Pleistocene-early Holocene Unit II (14–9.5 ka) (Figs. 5–6). The burial flux displays a similar trend of reduced accumulation in Units IA and IB (Fig. 7C). These temporal changes in the accumulation of TOC are not correlative to that of $CaCO_3$ burial flux changes – and inferred productivity – but rather follow lithogenic burial flux changes. This dataset is consistent with the hypothesis that organic matter deposited at MC118 is predominantly terrestrial in origin, or, at the very least, its burial is somehow influenced by greater terrigenous sedimentation linked to sea-level change and delta lobe switching (see below).

It has been suggested that the degree of organic matter oxidation and its preservation into the geologic record is proportional to the time spent within oxygenated sediments and associated aerobic decomposition (Hartnett et al., 1998). Then, it is also possible

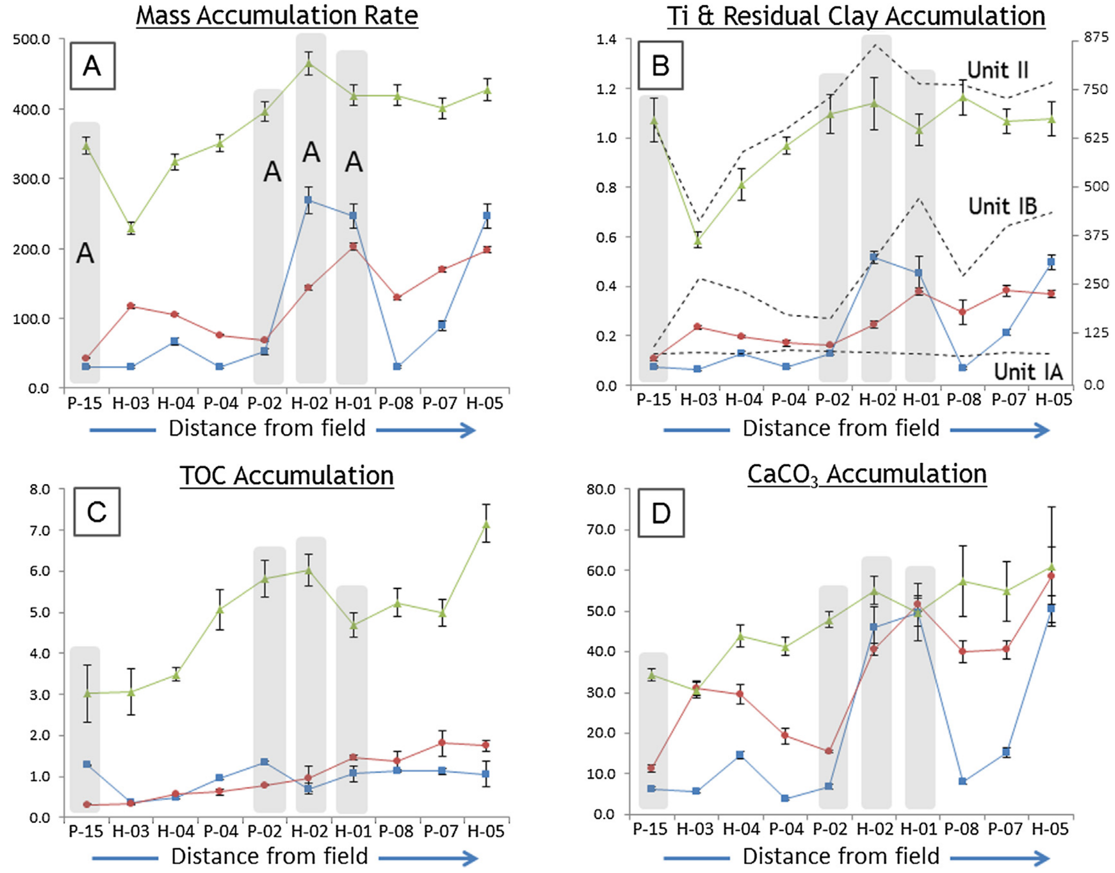

Figure 7. Mass accumulation rate (g m^{-2} yr^{-1}), along with Titanium (Ti), Total Organic Carbon (TOC), carbonate ($CaCO_3$), and insoluble residue (Residual Clay) accumulation rates calculated for each stratigraphic unit at each core site (Unit IA: blue, Unit IB: red and Unit II: green). The cores are arranged from left to right by increasing distance from the MC118 field (see Fig. 2) and are labeled on the *x*-axes to denote the cruise (P = Pelican and H = Hatteras) and core number. The shaded columns on each plot, labeled A on the top-left plot indicate core locations above the MC118 field. Errors are calculated using one standard deviation of duplicate measurements (XRF scans for Ti; CO_2 Coulometry for TOC, $CaCO_3$) and a chronologic error of 216 calendar years, the maximum error encountered from carbon-14 dating (Table 2 in Ingram et al., 2010). Error bars for residual clay (1 − $CaCO_3$ − TOC) are not calculated as respective errors are represented by other plots. Note the consistent increase of mass accumulation rate, Ti, TOC, and insoluble residue accumulation between Unit I (IA: blue, and IB: red) and Unit II (green), which is not replicated by $CaCO_3$ accumulation. (For interpretation of the references to color in this figure legend, the reader is referred to the web version of this article.)

that the observed increase in accumulation of organic matter in Unit II (Fig. 7C) is driven by rapid sedimentation (Fig. 7A), followed by slower accumulation in the later Holocene intervals (Ingram et al., 2010). This slower sediment accumulation during Units IA and IB may have provided sufficient time for organic matter to undergo greater aerobic decomposition, yielding lower present-day TOC concentration and a reduced burial flux (Figs. 5, 6 and 7C). However, changes in sedimentation rate alone are unlikely to account for the enhanced organic carbon burial flux at MC118. For instance, a 10-fold increase in sedimentation (open-marine setting) equates to a 2-fold increase in TOC (Müller and Seuss, 1979), yet MC118 displays a 2-fold increase in TOC (Figs. 5–6) and only a 2–3-fold increase in sedimentation (Ingram et al., 2010). Hence, this effect (a comparison of sedimentation rate to TOC concentration) is much more pronounced at MC118, or alternatively, some other mechanism is at work, such as a change in the composition of the organic matter.

To evaluate changes in the proportion of labile versus refractory organic matter though time, Rock Eval Pyrolysis results are presented using a Hydrogen Index (HI)-T_{max} cross-plot to determine kerogen type (Fig. 8). Kerogen is operationally defined as insoluble in organic solvents (Durand, 1980; Tissot and Welte, 1984), comprising a partially-converted, complex mixture of sedimentary organic matter, such as geopolymers (organic geomacromolecules) that have been subjected to early diagenesis (Schulz and Matthias, 2000). However, in very shallow sediments such as cores from MC118, this process is generally not complete. In these settings organic matter is only partially converted to kerogen, and the term "proto-kerogen" seems appropriate (Hollander et al., 1993). Holocene sediments spanning the seafloor to 55 cmbsf in Core HAT-03 plot in the mixed (proto)kerogen type II/III field, well above those from Unit II (below 55 cmbsf), which are found in the (proto)kerogen type III field on the cross-plot (Fig. 8). Thus, while allochtonous (terrigenous) organic matter is likely present throughout, the older Unit II sediments contain far more (proto)kerogen type III organics (Fig. 8), and at the same time greater lithogenic inputs (Figs. 3 and 7B). It seems likely that the (proto)kerogen type III signal is derived from terrestrial biogenic material eroded from the continent within the Mississippi River drainage basin.

It is also possible that organic matter at greater depth yields a lower hydrogen index due to selective biodegradation. In this scenario, hydrogen-rich (labile), organic matter is preferentially diminished with prolonged exposure to microbial decomposition, for instance Type I and II "proto-kerogens" can change their geochemical signal by moving down alteration pathways toward lower H/C and O/C ratios (Hollander et al., 1993). Thus, without changing the initial portion of marine to terrigenous organic matter reaching the seafloor, it may be possible to preserve more "refractory" organic matter and change the geochemical signal by this process. Additionally, it is also possible that the MC118 seep field

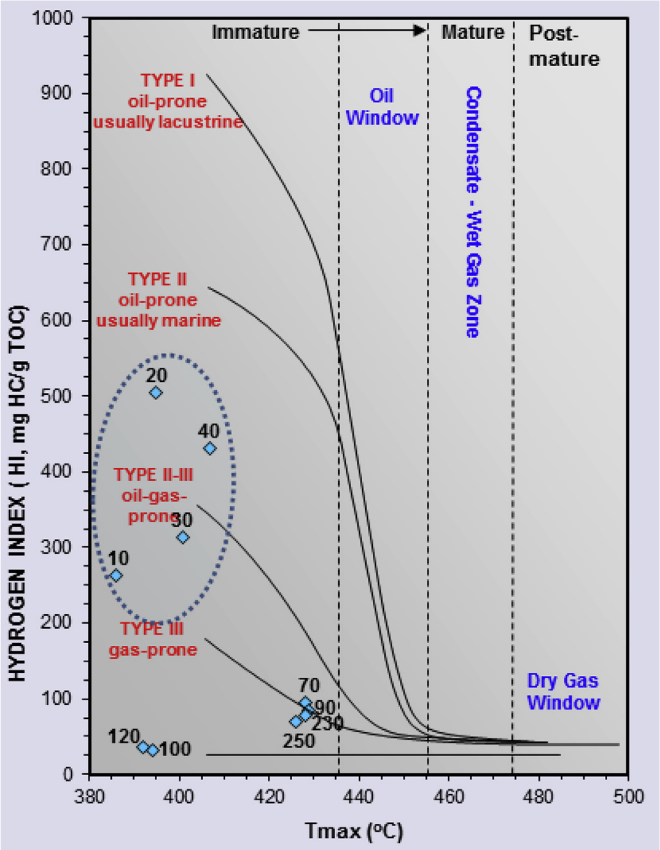

Figure 8. Rock Eval pyrolysis results from 10 samples of Core HAT-03 spanning Units I and II. Hydrogen Index (*y*-axis) plotted against T_{max} (*x*-axis) for each sample (blue diamonds). T_{max} (°C) is the temperature of maximum release of hydrocarbons from cracking of kerogens during pyrolysis (S_2 peak) and is an indication of maturation of the organic matter. All samples are immature, and thus plot left of the dashed lines. The hydrogen index is indicative of kerogen source, e.g. marine (oil prone) or terrestrial (gas prone), see discussion for interpretation. (For interpretation of the references to color in this figure legend, the reader is referred to the web version of this article.)

itself is a potential source of bitumen contributing to the surrounding MC118 sediments, thereby altering the geochemical signal, yet this is not apparent from pyrolysis data (lack of S1 peak). It also seems likely that tar deposits and/or authigenic carbonates would have been observed, yet there is no evidence for either based on sedimentological analysis of the cores (Ingram et al., 2010). If the Rock Eval results are interpreted as a degradation signal, this would suggest that Unit II sediments experienced greater degradation than Unit IA and IB, despite higher sedimentation rates. This observation is inconsistent with oxygen exposure time serving as the primary control on temporal changes in organic matter accumulation at MC118.

In conclusion, rock pyrolysis results are consistent with inorganic geochemistry (titanium and insoluble residue accumulation). Together, these results suggest terrigenous-dominated sedimentation characterizes the late Pleistocene-early Holocene (14–9.5 Ka) of Unit II, then transitioning to enhanced pelagic sedimentation during the early-mid Holocene (9.5–2.3 Ka). This is not surprising given the location of study area on the northern Gulf of Mexico slope, offshore from a major delta that was in closer proximity to MC118 during deposition of Unit II (a time of lower sea level). However, we cannot rule out the possibility that Unit II contains a higher proportion of degraded Type II organic matter, thereby resulting in lower hydrogen indices through organic matter alteration (Hollander et al., 1993).

5. Conclusions

This study reveals several key conclusions specific to the late Pleistocene to Holocene depositional history at MC118. The most important observation is that the flux of lithogenic inputs and organic carbon decreases with time (from the late Pleistocene to late Holocene), and burial rates for all components generally increases with greater distance from the gas hydrate and cold-seep field at each core site. Sediments shift from clay-rich during the late Pleistocene–earliest Holocene (14–9.5 Ka) to $CaCO_3$-rich during a period approximating the Holocene (9.5 Ka to present). This change is connected to post-glacial sea-level rise and proximity to the Mississippi delta, which are important controls on the delivery of terrigenous sediments to MC118. The mass accumulation rates of lithogenic proxies and Rock Eval data are consistent with an enhanced delivery of terrigenous organic matter during the late Pleistocene–earliest Holocene (14–9.5 Ka), a time of greater proximity of MC118 to terrigenous sources. In contrast, carbonate accumulation rates, and inferred carbonate productivity at MC118, show less pronounced temporal variability. Taken together, the new results suggest a complex depositional history at MC118, yet relatively stable spatial patterns of deposition around the nearby field, which reflect the salt diapir-induced bathymetric high that hosts present-day gas hydrates and cold seeps.

Acknowledgements

Financial support for this research was provided by university and departmental funds to Dr. Stephen Meyers (UNC-Chapel Hill and UW-Madison). Additional support was provided by the Gulf of Mexico Gas Hydrate Research Consortium (HRC grants 300212198E (UM 07-01-071) and 300212260E (UM 08-11-047) to C.S. Martens). Weatherford Geochemistry Lab in Houston Texas generated the Rock Pyrolysis data and supported the research by providing a discount to perform the analyses. Funding for ship time on the R/V Pelican was provided by Minerals Management Services (now Department of Ocean Energy) and NOAA's National Institute for Undersea Science and Technology. Funding for the R/V Hatteras Cruise, ship time and coring operations was provided by the Duke/UNC Oceanographic Consortium as part of a joint proposal with other UNC investigators, Kai Ziervogel, Drew Steen and Carol Arnosti. The crew, joint investigators listed above, Sherif Ghobrial, Carol Lutken and Ken Sleeper were all instrumental in the shipboard core collection process that provided the material used for this study. Finally, Dr. Thomas Pape provided very detailed and useful comments that greatly improved this manuscript.

References

Appelbaum, B.S., Bouma, A.H., 1972. Geology of the upper continental slope in the Alaminos Canyon region. Gulf Cost Association of Geological Societies Transactions 22, 157–164.
Bian, Y., Feng, D., Roberts, H.H., Chen, D., 2013. Tracing the evolution of seep fluids from authigenic carbonates: Green Canyon, northern Gulf of Mexico. Marine and Petroleum Geology 44, 71–81.
Bralower, T.J., Thierstein, H.R., 1987. Organic carbon and metal accumulation rates in Holocene and mid-Cretaceous sediments: paleoceanographic significance. In: Brooks, J., Fleet, A.J. (Eds.), Marine Petroleum Source Rocks, Geological Society of London Special Publication, vol. 26, pp. 345–369.
Claypool, G.E., Reed, P.R., 1976. Thermal analysis technique for source rock evaluation: quantitative estimate of organic richness and effects of lithologic variation. AAPG Bulletin 60, 608–626.
Corbett, R.D., McKee, B., Duncan, D., 2004. An evaluation of mobile mud dynamics in the Mississippi River deltaic region. Marine Geology 209, 91–112.
Dadey, K.A., Janecek, T., Klaus, A., 1992. Dry-bulk density: its use and determination. In: Proceedings of the Ocean Drilling Program, Scientific Results, vol. 126, pp. 551–554.

DeMaster, D.J., 1981. The supply and accumulation of silica in the marine environment. Geochimica et Cosmochimica Acta 45, 1715–1732.

Diegel, F.A., Karlo, J.F., Schuster, D.C., Shoup, R.C., Tauvers, P.R., 1995. Cenozoic structural evolution and tectono-stratigraphic framework of the northern Gulf Coast continental margin. In: Jackson, M.P.A., Roberts, D.G., Snelson, S. (Eds.), Salt Tectonics: a Global Perspective: American Association of Petroleum Geologist Memoir, vol. 65, pp. 109–151.

Durand, B., 1980. Kerogen. Insoluble Organic Matter from the Sedimentary Rocks? Editions Technip., Paris, p. 519.

Espitalié, J., Deroo, G., Marquis, F., 1985. La pyrolyse Rock-Eval et ses applications. Revue de l'Institut Francais du Petrole 40, 755–784.

Galloway, W.E., Ganey-Curry, P.E., Li, X., Buffler, R.T., 2000. Cenozoic depositional history of the Gulf of Mexico basin. American Association of Petroleum Geologist Bulletin 84 (11), 1743–1774.

Gordon, E.S., Goni, M.A., 2004. Controls on the distribution and accumulation of terrigenous organic matter in sediments from the Mississippi and Atchafalaya river margin. Marine Chemistry 92, 331–352.

Hartnett, H.E., Keil, R.G., Hedges, J.I., Devol, A.H., 1998. Influence of oxygen exposure time on organic carbon preservation in continental margin sediments. Nature 391, 572–574.

Hollander, D.J., McKenzie, J.A., Hsu, K.J., Huc, A.Y., 1993. Application of a eutrophic lake model to the origin of ancient organic-carbon-rich sediments. Global Biogeochemical Cycles 7, 157–179.

Huffman Jr., E.W.D., 1977. Performance of a new carbon dioxide coulometer. Microchemistry Journal 22, 567–573.

Ingram, W.C., Meyers, S.R., Brunner, C.B., Martens, C.S., 2010. Late Pleistocene–Holocene sedimentation surrounding an active seafloor gas-hydrate and cold-seep field on the Northern Gulf of Mexico Slope. Marine Geology 278, 43–53.

Jackson, M.P.A., 1995. Retrospective salt tectonics. In: Jackson, M.P.A., Roberts, D.G., Snelson, S. (Eds.), Salt Tectonics: a Global Perspective, AAPG Memoir, vol. 65, pp. 1–28.

Kasten, S., Freudenthal, T., Gingele, F.X., Schulz, H.D., 1998. Simultaneous formation of iron-rich layers at different redox boundaries in sediments of the Amazon deep-sea fan. Geochimica et Cosmochimica Acta 62 (13), 2253–2264.

Kujau, A., Nurnberg, D., Zielhofer, C., Bahr, A., Rohl, U., 2010. Mississippi River discharge over the last ~560,000 years. Indications from X-ray fluorescence core-scanning. Palaeogeography, Palaeoclimatology, Palaeoecology 298, 311–318. http://dx.doi.org/10.1016/j.palaeo.2010.10.005.

Lapham, L.L., Chanton, J.P., Martens, C.S., Higley, H., Jannasch, H.W., Woolsey, J.R., 2008. Measuring long term changes in dissolved ion and gas concentrations and stable isotopes at a hydrate site: Mississippi Canyon 118, Gulf of Mexico. Environmental Science and Technology 42, 7368–7373.

Lutken, C.B., Brunner, C.A., Lapham, L.L., Chanton, J.P., Rogers, R., Sassen, R., Dearman, J., Lynch, L., Kuykendall, J., Lowrie, A., 2006. Analyses of core samples from Mississippi Canyon 118, paper OTC 18208. In: Presented at the Offshore Technology Conference. American Association of Petroleum Geologist, Houston, TX.

Macelloni, L., Caruso, S., Lapham, L., Lutken, C., Brunner, C., Lowrie, A., 2010. Spatial distribution of seafloor bio-geological and geochemical processes as proxy to evaluate fluid-flux regime and time evolution of a complex carbonate/hydrates mound, northern Gulf of Mexico. Gulf Coast Association of Geological Societies Transactions 60, 461–480.

Macelloni, L., Simonetti, A., Knapp, J.H., Knap, C.C., Lutken, C.B., Lapham, L.L., 2012. Multiple resolution seismic imaging of a shallow hydrocarbon plumbing system, Woolsey Mound, Northern Gulf of Mexico. Marine and Petroleum Geology 38, 128–142.

Marchitto, T.M., Wei, K.-Y., 1995. History of the Laurentide meltwater flow to the Gulf of Mexico during the last deglaciation, as revealed by reworked calcareous nannofossils. Geology 23, 779–782.

McBride, B.C., 1998. The evolution of allochthonous salt along a megaregional profile across the northern Gulf of Mexico. AAPG Bulletin 82, 1037–1054.

McGee, T., 2006. A seafloor observatory to monitor gas hydrates in the Gulf of Mexico. The Leading Edge 25 (5), 644–647.

Müller, P.J., Seuss, E., 1979. Productivity, sedimentation rate, and sedimentary organic matter in the oceans – organic carbon preservation. Deep-Sea Research 26, 1347–1362.

Murray, R.W., Miller, D.J., Kryc, K.A., 2000. Analysis of Major and Trace Elements in Rocks, Sediments, and Interstitial Waters by Inductively Coupled Plasma-Atomic Emission Spectrometry (ICP-AES). ODP Technical Note, 29, [Online] Available from World Wide Web: http://www-opd.tamu.edu/publications/tnotes/tn29/INDEX.HTM [Cited 2002-07-23].

Pattan, J.N., Masuzawa, T., Borole1, D.D., Parthiban, G., Jauhari, P., Yamamoto, M., February 2005. Biological productivity, terrigenous influence and noncrustal elements supply to the Central Indian Ocean Basin: paleoceanography during the past » 1 Ma. Journal of Earth System Science 114 (1), 63–74.

Prather, B.E., Booth, J.R., Steffens, G.S., Craig, P.A., 1998. Classification, lithologic calibration, and stratigraphic succession of seismic facies of intra-slope basins, deep-water Gulf of Mexico. American Association of Petroleum Geologists Bulletin 82, 701–728.

Richter, et al., 2006. The Avaatech core scanner: technical description and applications to NE Atlantic sediments. In: Rothwell, R.G. (Ed.), New Ways of Looking at Sediment Core and Core Data, Geological Society Special Publication, London, pp. 39–50.

Sageman, B.B., Lyons, T.W., 2004. Geochemistry of fine-grained sediments and sedimentary rocks. In: MacKenzie, F. (Ed.), 2004. Sediments, Diagenesis, and Sedimentary Rocks, Treatise on Geochemistry, vol. 7, pp. 115–158.

Sassen, R., Roberts, H.H., Jung, W., Lutken, C.B., DeFreitas, D.A., Sweet, S.T., Guinasso Jr., N.L., 2006. The Mississippi Canyon 118 Gas Hydrate Site: a Complex Natural System. Paper OTC 18132 Presented at the Offshore Technology Conference, Houston, TX.

Schulz, H.D., Matthias, Z. (Eds.), 2000. Marine Geochemistry, vol. 1. Springer-Verlag, ISBN 3-540-66453-X, p. 455. DM149.

Simonetti, A., Knapp, J.A., Sleeper, K., Lutken, C.B., Macelloni, L., Knapp, C., 2013. Spatial distribution of gas hydrates from high-resolution seismic and core data, Woolsey Mound, Northern Gulf of Mexico. Marine and Petroleum Geology 44, 21–23.

Sleeper, K.A., Lutken, C., 2008. Activities Report for Cruise GOM1-08-MC118 Aboard the R/V Pelican Sampling and Deployment Cruise Mississippi Canyon Federal Lease Block 118 Northern Gulf of Mexico April 22–28, 2008. Supported by. Center for Marine Resources and Environmental Technology and Seabed Technology Research Center University of Mississippi.

Sleeper, K.A., Lowrie, A., Bosman, A., Macelloni, L., Swann, C.T., 2006. Bathymetric Mapping and High Resolution Seismic Profiling by AUV in MC 118 (Gulf of Mexico). Paper OTC 18133 Presented at Offshore Technology Conference, Houston, TX.

Snowdon, L.R., Meyers, P.A., 1992. Source and maturity of organic matter in sediments and rocks from Sites 759, 760, 761 and 764 (Wombat Plateau) and Sites 762 and 763 (Exmouth Plateau). In: von Rad, U., Haq, B.U., et al. (Eds.), Proceedings of the Ocean Drilling Program, Scientific Results, vol. 122, pp. 309–315.

Tissot, B.P., Welte, D.H., 1984. Petroleum Formations and Occurrences, second ed. Springer and Verlag, Berlin, p. 699.

Törnqvist, T.E., Wortman, S.R., Mateo, Z.R.P., Milne, G.A., Swenson, J.B., 2006. Did the last sea level lowstand always lead to cross-shelf valley formation and source-to-sink sediment flux? Journal of Geophysical Research 111, 1–13. F04002.

Winkler, C.D., 1996. High Resolution Seismic Stratigraphy of a Late Pleistocene Submarine Fan Pounded by Salt-withdrawal Mini-basins of the Gulf of Mexico Continental Slope: Offshore Technology Conference Proceedings, OTC 8024, pp. 619–628.

Winn Jr., R.D., Roberts, H.H., Kohl, B., Fillon, R.H., Bouma, A.H., Constans, R.E., 1995. Latest Quaternary deposition on the outer shelf, northern Gulf of Mexico: facies and sequence stratigraphy from the Main Pass Block 303 shallow core. Geological Society of America Bulletin 107, 851–866.

Woolsey, J.R., 1984. Exploration for Industrial Minerals in Mississippi Sound and Adjacent Offshore Territories of Mississippi and Alabama. Mississippi–Alabama Sea Grant Consortium, Project No. R/ER-11, Grant No. NA81AA-D-00050, p. 22.